


# Tunneling anisotropic magnetoresistance in MgO-based magnetic tunnel junctions induced by spin-orbit coupling

Hui-Min Tang<sup>1</sup>, Shi-Zhuo Wang<sup>2</sup>, and Xing-Tao Jia<sup>3,\*</sup>

<sup>1</sup>*School of Physical Science and Technology, Guangxi Normal University, Guangxi 541001, China*

<sup>2</sup>*School of Physics and Electronic Engineering, Zhengzhou University of Light Industry, Zhengzhou 450002, China*

<sup>3</sup>*School of Physics and Electronic Information Engineering, Henan Polytechnic University, Jiaozuo 454000, China*

 (Received 22 April 2022; revised 7 July 2022; accepted 29 August 2022; published 6 September 2022)

We performed a first-principles study of the tunneling anisotropic magnetoresistance (TAMR) in Ag(Ir,Pt)/MgO/Fe junctions. An enhanced TAMR of the order of 10% is found in the junctions at the equilibrium state, which shows ideal and skewed fourfold angular dependence for the in-plane and out-of-plane TAMR, respectively. The TAMR effect in the junctions shows a simple barrier thickness dependence with the largest TAMR effect present in the junction with an  $\sim 6$ -monolayer MgO barrier. The interfacial states due to the spin-orbit coupling effect should be responsible for the complex and enhanced TAMR effect found in these junctions. A little interfacial oxygen vacancy disorder at the Fe/MgO interface can noticeably deteriorate the TAMR effect.

DOI: [10.1103/PhysRevB.106.094406](https://doi.org/10.1103/PhysRevB.106.094406)

## I. INTRODUCTION

An anisotropic magnetoresistance (AMR) effect, which is less than 1% generally, was found in ferromagnetic alloys and normal metal/ferromagnet (NM/FM) interfaces and has been well understood for a long time. The weak AMR effect in these materials makes it hard for them to function well in spintronic applications. A successful method to enhance the AMR effect in the NM/FM interface is the introduction of a functional layer such as an insulator barrier [1–14]. Enhanced tunnel AMRs (TAMRs) ranging from 1 to 10% are reported [1–10]. At the same time, several reports found a giant TAMR larger than 100% [12–14]. A giant TAMR amounting to 150 000% at very low temperature was reported in (Ga,Mn)As/GaAs/(Ga,Mn)As junctions [12]; the metal-insulator transition induced by the spin-orbit coupling (SOC) effect makes the giant TAMR effect drastically sensitive to the ambient temperature. An  $\sim 500\%$  TAMR is predicted in a  $\text{La}_{0.7}\text{Sr}_{0.3}\text{MnO}_3$  (LSMO) based tunnel junction [13], which originates from the half-metallic nature of the LSMO electrodes and the presence of quasilocalized interface states which are spin-orbit coupled. An unusual TAMR effect larger than 100% at 4 K was reported in an NiFe/IrMn/MgO/Pt spin-valve-like structure, which is reduced by a few percent at higher temperature unfortunately [14].

Surface states play an important role in the tunnel magnetoresistance (TMR) effect in the Fe/vacuum/Fe magnetic tunnel junction [15], which can enhance the Rashba SOC effect and enhance the TAMR effect [7,8]. Chantis *et al.* [7] predicted a TAMR of up to 20% in an Fe/vacuum/Cu junction at small bias voltages. Hervé *et al.* [8] found a TAMR of up to 30% in thick hcp Co films using scanning tunneling

microscopy and considered the strong TAMR as originating from the coupling of the surface state and the bulk state. However, when the sandwiched vacuum layer is replaced by a solid insulator, the TAMR effect seems to deteriorate [1–10]. Recently, Gao *et al.* [9] found a TAMR of  $\sim 1\%$  in the FeCo/MgO/FeCo and FeCo/Al<sub>2</sub>O<sub>3</sub>/FeCo magnetic tunnel junctions (MTJs) with crystalline MgO and an amorphous Al<sub>2</sub>O<sub>3</sub> barrier. Both junctions show complex angular dependence with strong sensitivity to bias voltage, and the former shows fourfold angular dependence while the latter shows twofold. The fourfold angular dependence therein is explained by the coupling of the interfacial resonant states (IRSs) with the interfacial density of states of the majority band. IRSs in the one ferromagnetic lead junction can be noticeable also. A recent study predicted a large mixing conductance in an Ag/MgO/Fe junction [16], which is caused by the IRSs. Following the scheme described in Ref. [9], we can speculate that there is a considerable TAMR effect in the Ag/MgO/Fe junction.

Here, we carry out first-principles calculations on the spin transport in the NM/MgO/Fe junctions to investigate the TAMR effect, where NM stands for Ag, Pt, and Ir. We found a noticeable TAMR effect in these junctions, where the in-plane TAMR shows an ideal fourfold angular dependence while the out-of-plane TAMR shows a skewed fourfold angular dependence. The complex angular dependence of the interfacial states due to the SOC effect should be responsible for the complex and enhanced TAMR effect found in these junctions.

This paper is organized as follows. In Sec. II, we introduce two configurations of TAMR: the in-plane and out-of-plane configurations. In Sec. III, we present our results of the TAMR in the NM/MgO/Fe MTJs and provide a systematic discussion of the relation of the angular dependence of the TAMR and the interfacial states. Moreover, the effect of the thickness of the tunnel barrier and the effect of oxygen vacancies at

\*Corresponding author: [jiayingtao@hpu.edu.cn](mailto:jiayingtao@hpu.edu.cn)

the Fe/MgO interface on the TAMR effect are discussed also. Section IV is our summary.

## II. METHODS

According to the structure of the NM/MgO/Fe(001) junctions (NM = Ag, Ir, and Pt) considered in our calculations, two magnetic structures should be considered for the TAMR effect; they are the in-plane and out-of-plane structures. The former refers to the Fe magnetization rotated within the  $x$ - $y$  plane, while the latter refers to the Fe magnetization rotated within planes perpendicular to the  $x$ - $y$  plane, with  $z$  along the epitaxial direction. The in-plane and out-of-plane TAMRs are defined as [6,17]

$$\text{TAMR}^{\text{in}}(90, \phi) = \frac{G(90, \phi) - G(90, 0)}{G(90, 0)}, \quad (1)$$

$$\text{TAMR}^{\text{out}}(\theta, \phi) = \frac{G(\theta, \phi) - G(0, 0)}{G(0, 0)}, \quad (2)$$

where  $G(\theta, \phi)$  denotes the tunneling conductance of the structure with the Fe magnetization along the direction defined by the unit vector  $\mathbf{m} = (\sin \theta \cos \phi, \sin \theta \sin \phi, \cos \theta)$ , where the units of the azimuth angles are degrees.

For the NM/MgO/Fe junctions considered here, bcc Fe with crystal constant  $a_{\text{Fe}} = 2.866 \text{ \AA}$  is chosen as the right lead, the sandwiched MgO is reduced and rotated  $45^\circ$  to match with the bcc Fe, and the left lead, NM, is compressed in the lateral direction and expanded in the transport direction to match with the MgO/Fe bilayer. The structural details of the MgO/Fe interface can be found in Ref. [18]. For the NM/MgO interface, the NM atom is sited above the O atom of the sandwiched MgO. The atomic sphere radii are 1.584, 1.534, and 1.500  $\text{\AA}$  for Ag, Ir, and Pt, respectively, whose spaces fill their fcc lattice. For the Ag/MgO interface, two vacuum spheres are inserted exactly above the vacuum spheres inside the MgO with the same radius, and a vacuum sphere of radius 0.872  $\text{\AA}$  is added exactly above the Mg atom to fill the total volume, corresponding to a distance  $d_{\text{Ag-MgO}} = 2.52 \text{ \AA}$  [19]. For the Ir/MgO and Pt/MgO interfaces, we expand the NM in plane to match with the MgO/Fe bilayer and compress the NM out of plane to keep their bulky volume, and we keep their interfacial structure the same as that of the Ag/MgO bilayer. More details on the structure can be found in Ref. [16]. We set the electronic current along the epitaxial direction, and we set the quantum axis along the epitaxial direction also. A  $400 \times 400$   $k$ -point mesh is used in the two-dimensional Brillouin zone (2D BZ) to ensure numerical convergence. For the disordered-interface case, we use a  $40 \times 40$   $k$ -point mesh in the full two-dimensional BZ for a  $5 \times 5$  lateral supercell, and six configurations are used to ensure configuration convergence. The scattering matrix was obtained using a first-principles wave function match (WFM) method [20,21] with tight-binding linearized muffin-tin orbitals (TB-LMTOs) [22,23] including the SOC effect [24–26] via the perturbation method.

## III. TAMR IN NM/MgO/Fe JUNCTIONS

Figure 1 shows the angular dependence of the TAMR of Ag/MgO/Fe junctions with a three-monolayer (3-ML;

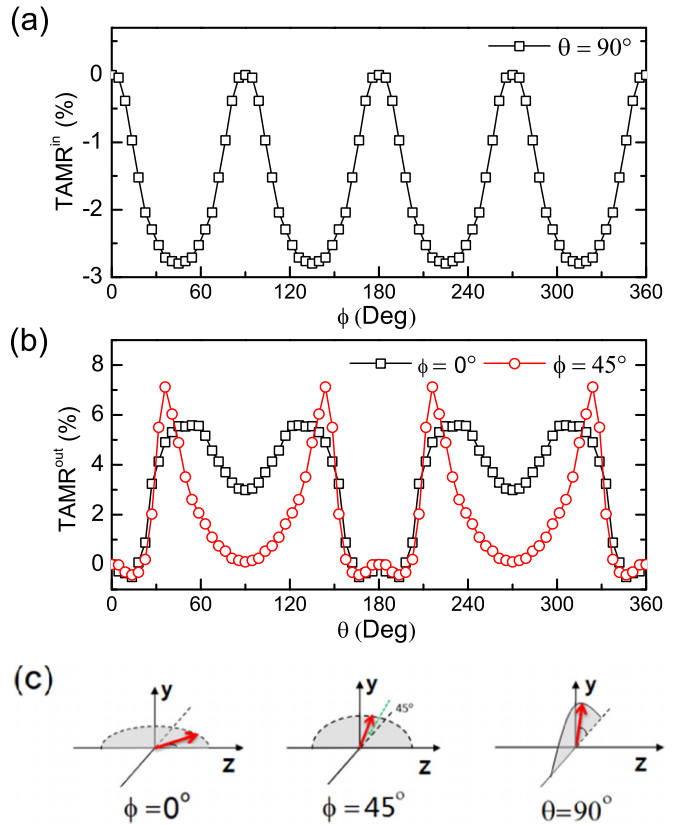


FIG. 1. Angular-dependent (a) in-plane and (b) out-of-plane TAMR of a clean Ag/MgO(3 ML)/Fe junction. (c) Schematic pictures of the rotation of the Fe magnetization.

3 MLs  $\sim 6 \text{ \AA}$ ) MgO barrier with a clean interface. We consider three magnetic structures with the Fe magnetization rotating within the  $x$ - $z$ ,  $(1\bar{1}0)$ , and  $x$ - $y$  planes, respectively, corresponding to  $\phi = 0^\circ$ ,  $\phi = 45^\circ$ , and  $\theta = 90^\circ$ , respectively, as sketched in Fig. 1(c). The first one shows the in-plane structure, while the last two show the out-of-plane structure.

Ideal fourfold angular-dependent in-plane TAMR close to a trigonometric function is found in the junction with in-plane structure, as shown in Fig. 1(a), which shows a negative TAMR with maximum conductances present at  $\phi = 0^\circ, 90^\circ, 180^\circ,$  and  $270^\circ$  and minimum conductance at  $\phi = 45^\circ, 135^\circ, 225^\circ,$  and  $315^\circ$ , which is almost equal to the conductance of the junction with Fe magnetization along the  $[001]$  direction. This is consistent with previous studies [27]. Comparatively, skewed fourfold angular-dependent out-of-plane TAMR is found in the junctions with out-of-plane structures as shown in Fig. 1(b), which is almost antiphase with the in-plane TAMR of the junction with in-plane structure. Sharp peaks with a value around 0.08 at  $\phi = 35^\circ, 145^\circ, 215^\circ,$  and  $325^\circ$  are found in the out-of-plane TAMR( $\theta, 45^\circ$ ). At the same time, the out-of-plane TAMR( $\theta, 0$ ) is relatively smooth. Both out-of-plane structures show small ghost valleys around  $\phi = 0^\circ$  and  $180^\circ$ .

To understand the angular dependence of TAMR as shown in Fig. 1, we plot firstly the  $k_{\parallel}$ -resolved transmission at the Fermi energy  $E_F$  for the clean Ag/MgO(3 ML)/Fe junction, as shown in Figs. 2(a)–2(e). Therein,  $k_{\parallel}$  points near the  $\Gamma$  point contribute mainly to the total transmission, accompanied

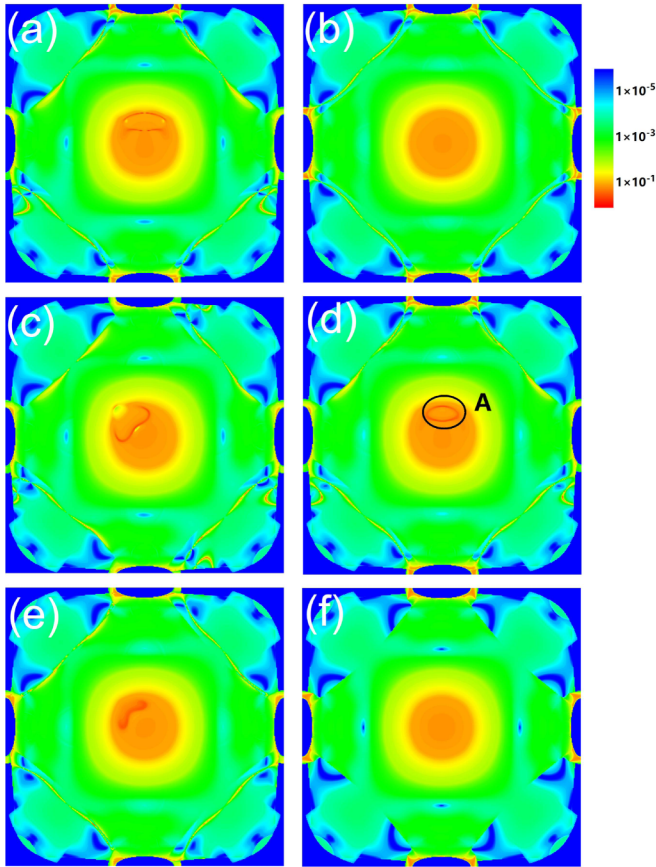


FIG. 2.  $k_{\parallel}$ -resolved electron transmission of the clean Ag/MgO(3 ML)/Fe junction. The Fe magnetization is along the (a) [100], (b) [001] ( $z$ ), (c) [110], (d)  $\theta = 54^\circ$  and  $\phi = 0^\circ$ , and (e)  $\theta = 36^\circ$  and  $\phi = 45^\circ$  directions. (f)  $k_{\parallel}$ -resolved electron transmission of the junction as the SOC effect is turned off.

by several continuous hot lines close to the  $\Gamma$  point, some hot  $k_{\parallel}$  points in series, and several small hot spots near the edge of the BZ. The hot spots, points, and lines are from the  $d$  electrons at the Fermi level energy; most of the former two and all of the latter disappear when the SOC effect is turned off, as shown in Fig. 2(f). All the hot spots, points, and lines are sensitive to the magnetization direction, as shown in Figs. 2(a)–2(e), which would experience a continuous or sharp change as the magnetization direction rotates. This indicates that the SOC effect in the Ag/MgO(3 ML)/Fe junction is highly angular dependent, and the SOC-effect-induced interface electronic structure should be the origin of the TAMR effect.

Among all the magnetic structures listed in Figs. 2(a)–2(e), the structure with Fe magnetization along the  $z$  axis shows a less hot transmission area, and the total transmission summed within the 2D BZ is noticeably smaller than that of the other structures. The  $k_{\parallel}$ -resolved transmission shows mirror symmetry in the 2D BZ when the Fe magnetization deviates from the quantum axis, while highly rotational symmetry with an order of 4 is present when the Fe magnetization is along the quantum axis. The total transmission of the structure with Fe magnetization along the  $x$  axis is equal to that of the structure with Fe magnetization along the  $y$  axis, and a  $90^\circ$

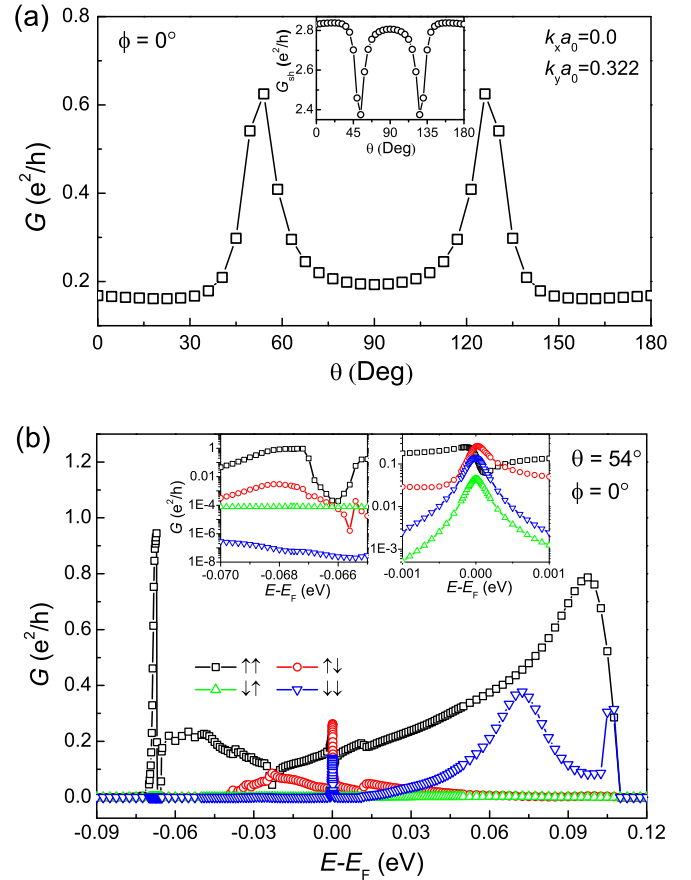


FIG. 3. (a) Angular-dependent transmission of the clean Ag/MgO(3 ML)/Fe junction at the  $k_x a_0 = 0.0$  and  $k_y a_0 = 0.322$  point, where  $a_0 = 0.286$  nm is the lattice constant of bcc Fe. Inset: Sharvin transmission of bcc Fe at the same  $k_{\parallel}$  point. (b) Energy-dependent spin transmission at the same  $k_{\parallel}$  point with Fe magnetization along  $\theta = 54^\circ$  and  $\phi = 0^\circ$ . Insets: Enlargement images.

rotation of the former would get the latter; this is consistent with the fourfold angular dependence of the in-plane TAMR of the junction. The symmetry of the magnetic structure and the SOC effect (including both the Dresselhaus SOC and Bychkov-Rashba SOC effect) [6] should be accounted for. Though the  $k_{\parallel}$ -resolved transmission of the structure with Fe magnetization along [110] is noticeably different from that along the  $z$  axis, the enhanced hot lines close to the  $\Gamma$  point in the former cancel the weakened hot spots at the edge and hot points in series. As a result, the two structures show almost equal total conductance.

Figure 2(d) shows the  $k_{\parallel}$ -resolved transmission of the clean Ag/MgO(3 ML)/Fe junction with the Fe magnetization along  $\theta = 54^\circ$  and  $\phi = 0^\circ$ . In this figure, the most obvious feature is the hot circle formed close to the  $\Gamma$  point, which is evolutive from several hot lines in the structure with Fe magnetization along the  $z$  axis. The hot line close to the  $\Gamma$  point of the structure with Fe magnetization along  $\theta = 36^\circ$  and  $\phi = 45^\circ$  is getting thicker compared with that of the structure with Fe magnetization along [110]. It is hard to distinguish the effect of SOC on the Sharvin conductance of the bcc Fe lead, not only from the  $k_{\parallel}$ -resolved transmission but also from the



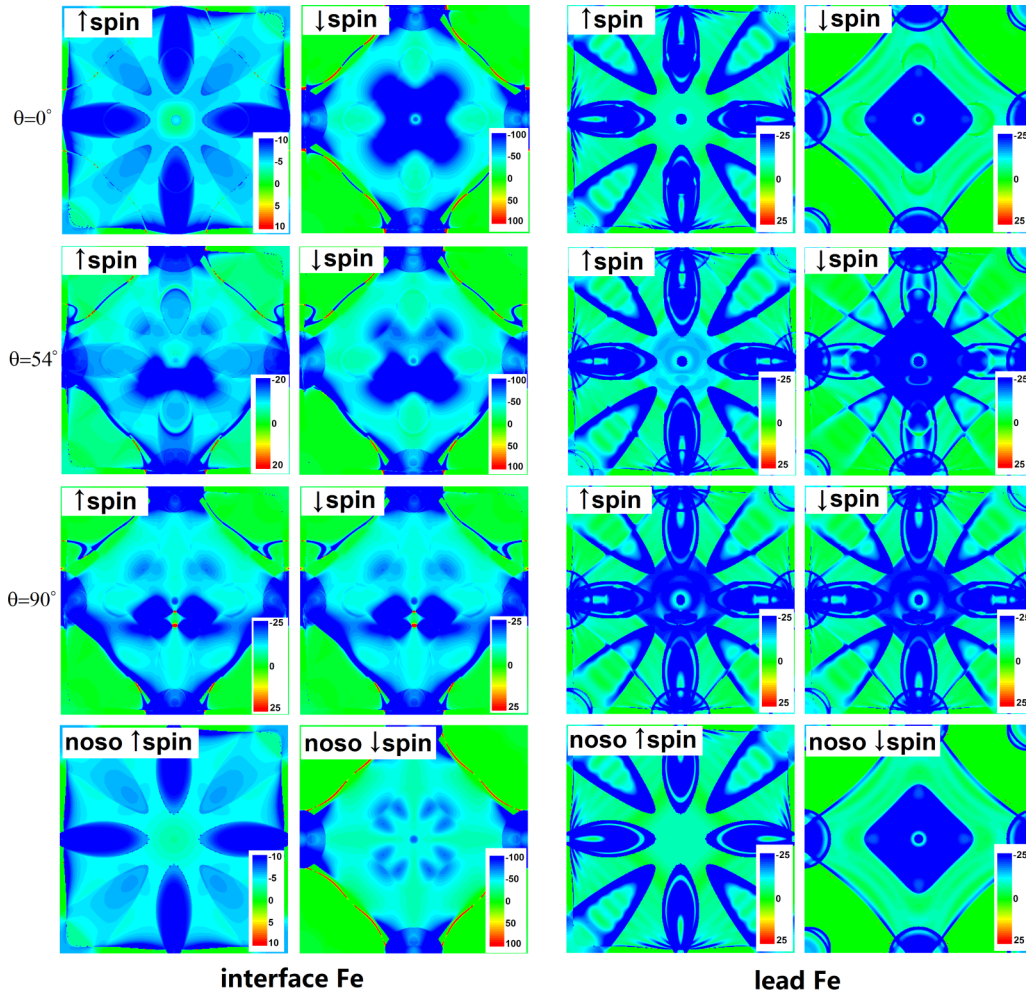


FIG. 4.  $k_{\parallel}$ -resolved charge density of the Fe atom at the MgO/Fe interface and of the tenth Fe atom from the interface of the clean Ag/MgO(3 ML)/Fe junctions with Fe magnetization rotated within the  $x$ - $z$  plane. Here, we refer to these Fe atoms as the interface Fe and lead Fe, respectively. In this figure, the positive and negative values indicate the right- and left-going spin density, respectively. As a comparison, the charge density of interface Fe and lead Fe atoms in the junction in the absence of the SOC effect [no SOC (noso)] is given in the bottom row, also.

total conductance, which indicates that the hot regions shown in Figs. 2(a)–2(e) are dominated by the interfaces. Further calculations in the absence of the SOC effect in the leads demonstrate these points. Not only the convergency but also the calculation consummation are considerably improved as the SOC effect in leads is turned off.

Let us focus on a high-transmission  $k_{\parallel}$  point with  $k_x a_0 = 0.0$  and  $k_y a_0 = 0.322$  on the ring labeled “A” of the clean Ag/MgO(3 ML)/Fe junctions with Fe magnetization along  $\theta = 54^\circ$  and  $\phi = 0^\circ$ , as shown in Fig. 2(d). Therein, we find that both the angular-dependent conductance and the energy-dependent conductance of the  $k_{\parallel}$  point are sensitive to the direction of Fe magnetization; as shown in Fig. 3, this indicates the formation of interface states. The angular-dependent Sharvin conductance of the  $k_{\parallel}$  point is sensitive to the direction of Fe magnetization also, as shown in the inset of Fig. 3(a), which is almost antiphase with the angular-dependent conductance, with the peak value around  $\theta = 54^\circ$ . The noninteger Sharvin conductance indicates a considerable Dresselhaus SOC effect in the bulk bcc Fe, which is almost buried when the sum is taken within the full 2D BZ. There are

four peaks present in the energy-dependent spin transmission of the  $k_{\parallel}$  point as shown in Fig. 3(b), with two sharp peaks and two smooth peaks. The sharp peak around the Fermi level is related to the interfacial states in the minority  $\downarrow$  band, while the sharp peak around 0.068 eV below the Fermi level is related to the interfacial states in the majority  $\uparrow$  band. The two sharp peaks are from different bands, indicating the formation of interface states at the Fe/MgO interfaces rather than interface resonance formed across the sandwiched MgO, where the bonding and antibonding peaks are always closely adjacent. Moreover, sharp peaks indicate that the interfacial states are highly localized. The two smooth peaks around 0.07 and 0.1 eV above the Fermi level are from the  $\uparrow$  and  $\downarrow$  band, respectively, which should be related to the entrance of two new Bloch states.

The SOC effect should change the charge density. So the atomic-resolved charge density can be used to explain the effect of SOC on the transmission. Figure 4 shows the  $k_{\parallel}$ -resolved charge density of interface Fe of the clean Ag/MgO(3 ML)/Fe junctions with Fe magnetization rotated within the  $x$ - $z$  plane. Therein, the  $k_{\parallel}$ -resolved charge den-

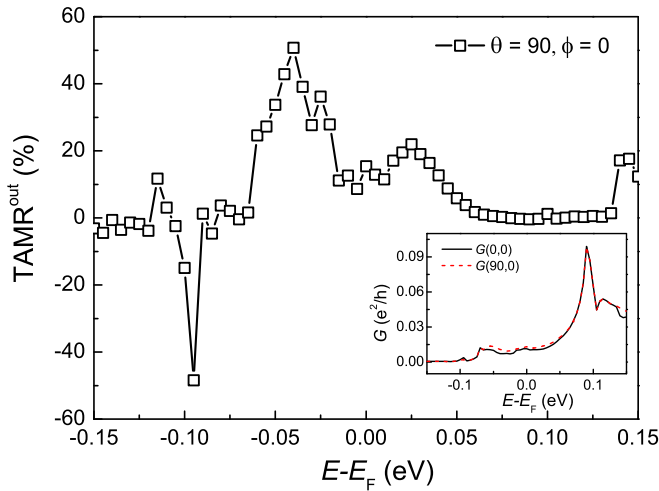


FIG. 5. Energy dependence of the TAMR<sup>out</sup> of the clean Ag/MgO(3 ML)/Fe junction. Inset: Energy dependence of the conductances.

sity of the lead Fe, as shown in the right two columns of Fig. 4, is almost angular independent and looks similar to the  $k_{\parallel}$ -resolved Sharvin conductance. As  $\theta$  increases from  $0^{\circ}$  to  $90^{\circ}$ , the charge density of the interface Fe changes from rotation symmetry with an order of 4 to mirror symmetry. Both the  $\uparrow$  spin and the  $\downarrow$  spin are noticeably changed as the angle changes. The charge density of the lead Fe atom is weakly angular dependent, demonstrating a weak SOC effect in the leads. Moreover, both the left- and right-going charge densities of the interface Fe are asymmetric; this indicates that the left-going SOC effect is different from the right-going SOC effect, leading to noticeable asymmetry in the voltage-bias-dependent transmission. Moreover, the strong angular dependence in the right- and left-going charge densities means that the voltage-bias-dependent magnetic Gilbert damping is possibly enhanced by the SOC effect.

The angular dependence of the band structure of the interface Fe atom is analyzed to further understand the angle dependence of the tunneling conductance. In this analysis, the potential of the interface Fe atom is placed on a perfect bcc lattice, and the band structure is non-self-consistently calculated. The SOC effect opens the degenerate band with a gap around 0.12 eV near the Fermi level as the Fe magnetization is along the  $z$  axis. This gap shrinks as the Fe magnetization rotates from the  $z$  axis to the  $x$  axis, and finally a crossing point is reached. This is consistent with recent research [25]. The AMR effect within the  $x$ - $z$  plane contributed from the SOC band structure of the interfacial Fe atom follows a twofold angular dependence with the largest value being  $\sim 2\%$  [25], which is about one order of magnitude smaller than that from the interfacial SOC effect in these calculations.

As discussed above, though the spin transmission from the interfacial states is sensitive to the energy, the sum of them in the 2D BZ is insensitive to the energy as shown in the inset of Fig. 5. We observe positive out-of-plane TAMR with values ranging from 10 to 50% within the energy range from  $E_F - 0.05$  eV to  $E_F + 0.05$  eV with a peak value of  $\sim 50\%$  around  $E_F - 0.04$  eV in the clean Ag/MgO(3 ML)/Fe junction.

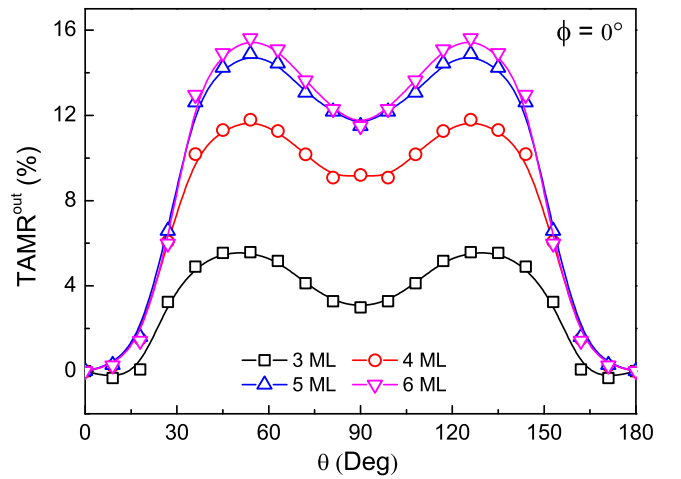


FIG. 6. Angular dependence of the out-of-plane TAMR of the clean Ag/MgO( $x$  ML)/Fe junctions.

Moreover, negative out-of-plane TAMR with a peak value of approximately  $-50\%$  is shown around  $E_F - 0.095$  eV. Though noticeable out-of-plane TAMR is present within a large range of energy, the bias-voltage-dependent TAMR can show a different behavior for the complex coupling between the interfacial states and the bias voltage [9,28]. That is, the angular dependence of the TAMR at a larger bias voltage can be considerably different from that at the equilibrium state [9].

It is well known that a thicker MgO barrier can enhance the spin-filtering effect in the MgO-based MTJs [18,29]. If both the spin-filtering effect and the interfacial SOC effect share the same  $k_{\parallel}$  points in the 2D BZ, their coupling might enhance the AMR effect further. Figure 6 shows the angular dependence of the out-of-plane TAMR of clean Ag/MgO/Fe junctions as a function of the thickness of the MgO barrier. Although the tunneling conductance decreases, the out-of-plane TAMR increases as the thickness of the MgO layer increases from 3 MLs to 6 MLs, which shows a quick increment at first and then gets to saturation. The largest out-of-plane TAMR is shown within the range from  $\theta = 45^{\circ}$  to  $60^{\circ}$  with a peak value of around 15% in a 6-ML MgO junction. The out-of-plane TAMR( $90, 0$ ) amounts to 12% for a 6-ML MgO junction. Further increasing the thickness of the MgO barrier shows less effect on the TAMR effect.

Table I summarizes the TAMRs of the clean Ag/MgO( $x$  ML)/Fe junctions discussed in this paper. Here, the maximum TAMR is defined as  $\text{TAMR}(\text{max}) = \frac{G(\text{max}) - G(\text{min})}{G(\text{min})}$ , with  $G(\text{max})$  being the maximum conductance and  $G(\text{min})$  being the minimum conductance, which is different from Eq. (2). For the junction with a 3-ML MgO barrier, the maximum in-plane TAMR is around 2.88%, which is considerably smaller than the maximum out-of-plane TAMR of 7.09% as the Fe magnetization is rotating within the  $(1\bar{1}0)$  plane. A larger TAMR(max) is present in the thicker-MgO-barrier junctions than in the thinner-barrier ones, and the largest TAMR(max) found in this paper amounts to 15.3% in a junction with a 6-ML MgO barrier (about 1.2 nm), which is one order of magnitude larger than the AMR effect in the single NM/FM interface.

TABLE I. TAMR of clean Ag/MgO( $x$  ML)/Fe junctions. The second column is the rotation plane of the Fe magnetization  $\mathbf{M}$ .  $G(\max)$  is the maximum of conductance as  $\mathbf{M}$  rotates, with the unit of conductance being  $10^{-3}e^2/h$ . The largest TAMR,  $\text{TAMR}(\max) = \frac{G(\max) - G(\min)}{G(\min)}$ , is defined, with  $G(\min)$  being the minimum conductance. The  $G(\min)$  is along  $\theta = 90^\circ$  and  $\phi = 45^\circ$  and along the  $z$  axis for the in-plane and out-of-plane structure, respectively.

$x$	Rotation plane	$G(\min)$	$G(\max)$	TAMR(max) (%)
3	$x$ - $y$	12.85	13.22	2.88
	$x$ - $z$	12.84	13.56	5.61
	( $\bar{1}\bar{1}0$ )	12.84	13.75	7.09
4	$y$ - $z$	2.015	2.253	11.8
5	$y$ - $z$	0.402	0.462	14.9
6	$y$ - $z$	0.085	0.098	15.3

Furthermore, the angular dependence of the TAMR in NM/MgO/Fe junctions when two different noble metals, Ir and Pt, serve as capping layers is estimated. Figure 7 shows the angular dependence of the out-of-plane TAMR of the Ir/MgO(3 ML)/Fe and Ir/MgO(3 ML)/Fe junctions with a clean interface. A similar skewed fourfold angular dependence was shown in the two junctions with TMAR(max) being about several percent larger than that in the Ag/MgO(3 ML)/Fe junctions. Two points are related to the enhanced TAMR effect in the Ir- and Pt-based junctions compared with the Ag-based junction. One is the larger SOC effect in Ir and Pt compared with Ag, and the other is related to the larger kinetic energy of the  $\Delta_1$  state in Ir and Pt compared with Ag. It is well understood that the  $\Delta_1$  state dominates the conductance in MgO-based junctions. Because

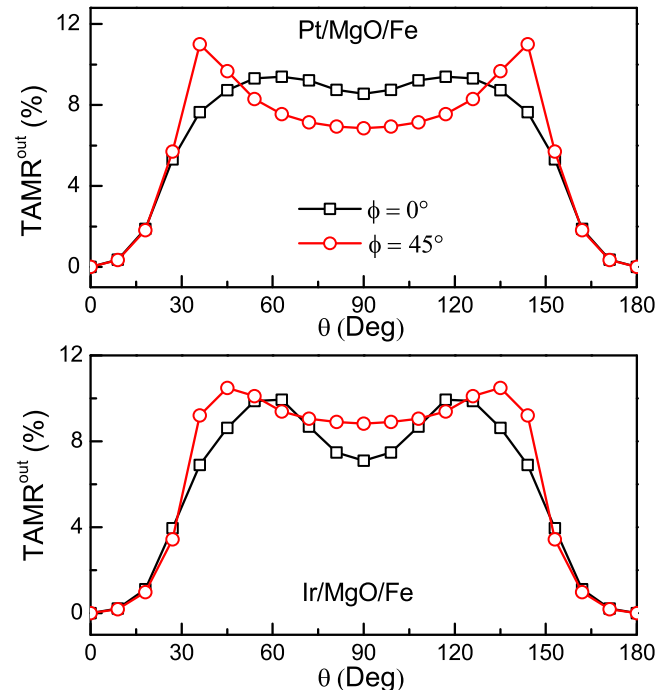


FIG. 7. Angular dependence of the out-of-plane TAMR of clean Pt/MgO(3 ML)/Fe and Ir/MgO(3 ML)/Fe junctions.

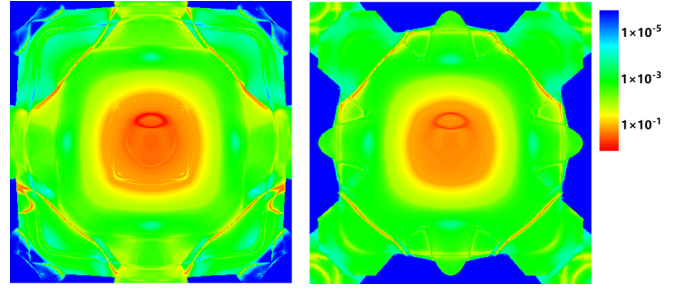


FIG. 8.  $k_{\parallel}$ -resolved electron transmission of the clean Pt/MgO(3 ML)/Fe (left) and Ir/MgO(3 ML)/Fe (right) junctions. The Fe magnetization is along the  $\theta = 54^\circ$  and  $\phi = 0^\circ$  direction.

the kinetic energy of the  $\Delta_1$  state in Ir and Pt is larger than in Ag at the Fermi energy [16], the conductances in Ir/MgO/Fe and Pt/MgO/Fe junctions are larger than that in Ag/MgO/Fe in both the case where the SOC effect is present and the case where the SOC effect is absent. Figure 8 gives the  $k_{\parallel}$ -resolved electron transmission of the clean Pt/MgO(3 ML)/Fe and Ir/MgO(3 ML)/Fe junctions with  $\theta = 54^\circ$  and  $\phi = 0^\circ$ . Therein, the bright spots and lines follow the same pattern as in the Ag/MgO(3 ML)/Fe junction. The brighter resonant spots and lines in the Ir- and Pt-based junctions indicate that the second point discussed above should be contributing mainly to the enhanced TAMR therein. Similar to the Ag/MgO/Fe junctions, thicker-MgO-barrier junctions show a larger TAMR effect in both Ir- and Pt-based junctions. Large out-of-plane TAMR(max) values amounting to 15.8 and 18.5% are found in the clean Pt/MgO/Fe and Ir/MgO/Fe junctions with a 6-ML MgO barrier.

We further studied the out-of-plane TAMR in NM/MgO(3 ML)/Fe (NM = Ag, Pt, or Ir) junctions with 4% oxygen vacancies (OVs) at the Fe/MgO interface with the Fe magnetization rotation within the  $x$ - $z$  plane. Therein, the out-of-plane TAMR shows a fourfold angular dependence similar to that found in the clean junctions. The out-of-plane TAMR(max) is about 5, 5.5, and 7% in a NM/MgO(3 ML)/Fe junction, where NM is Ag, Pt, and Ir, respectively, and the out-of-plane TAMR(90, 0) is about 1, 1.5, and 2.2%, respectively. Both sets of numbers are noticeably reduced when compared with the clean junctions. Introducing OVs into the Fe/MgO interface would deteriorate the interface states, cause the transmission channels to spread much more widely into the BZ, and then lead the spin transport from the specular scheme to the diffusive scheme [18]. Because the interface resonant tunneling is restrained in the presence of oxygen vacancy, the SOC-induced TAMR effect is restrained greatly in the dirty junction. So, to get a larger TAMR effect, the interface should be as clean as possible.

#### IV. SUMMARY

We performed a first-principles study of the TAMR effect in NM/MgO/Fe junctions. We found enhanced TAMR with fourfold angular dependence in these junctions with a value one order of magnitude larger than that for a NM/FM interface at the equilibrium state. The angular-dependent charge

density of the interface Fe should be responsible for the TAMR effect, which originates from the interfacial states in the presence of the SOC effect. Considering that the interfacial states are more prevalent than the interfacial resonant states, the enhanced AMR effect may exist more widely in multilayered heterostructures, because the former can exist in one single interface while the latter exist in multilayered heterostructures with two or more interfaces. Due to the larger kinetic energy of the  $\Delta_1$  state in Ir and Pt compared with Ag, we predict an enhanced TAMR effect in Ir/MgO/Fe and Pt/MgO/Fe junctions compared with that in the Ag/MgO/Fe junction. The MgO barrier thickness dependency of the TAMR effect in the junctions shows saturation at around six monolayers with a peak value of around 15%. An

interfacial oxygen vacancy at the Fe/MgO interface of several percent can change the spin transport from the specular scheme to the diffusive scheme, leading to a sharp decrease in the TAMR effect.

#### ACKNOWLEDGMENTS

We gratefully acknowledge financial support from the National Natural Science Foundation of China (Grants No. 11804062, No. 12074102, and No. 11804310), the National Key Research and Development Program (Grant No. 2018YFB0407600), and the Natural Science Foundation of Guangxi (Grant No. 2018GXNSFAA138160).

- 
- [1] T. V. Pham, S. Miwa, and Y. Suzuki, *J. Electron. Mater.* **45**, 2597 (2016).
- [2] N. Néel, S. Schröder, N. Ruppelt, P. Ferriani, J. Kröger, R. Berndt, and S. Heinze, *Phys. Rev. Lett.* **110**, 037202 (2013).
- [3] K. Wang, T. L. A. Tran, P. Brinks, J. G. M. Sanderink, T. Bolhuis, W. G. van der Wiel, and M. P. de Jong, *Phys. Rev. B* **88**, 054407 (2013).
- [4] J. Huangfu, C. Zhao, J. Zhang, B. Li, and G. Yu, *J. Appl. Phys.* **111**, 123903 (2012).
- [5] H. Saito, S. Yuasa, and K. Ando, *Phys. Rev. Lett.* **95**, 086604 (2005).
- [6] A. Matos-Abiague and J. Fabian, *Phys. Rev. B* **79**, 155303 (2009).
- [7] A. N. Chantis, K. D. Belashchenko, E. Y. Tsymbal, and M. van Schilfgaarde, *Phys. Rev. Lett.* **98**, 046601 (2007).
- [8] M. Hervé, T. Balashov, A. Ernst, and W. Wulfhekel, *Phys. Rev. B* **97**, 220406(R) (2018).
- [9] L. Gao, X. Jiang, S.-H. Yang, J. D. Burton, E. Y. Tsymbal, and S. S. P. Parkin, *Phys. Rev. Lett.* **99**, 226602 (2007).
- [10] M. Khan, J. Henk, and P. Bruno, *J. Phys.: Condens. Matter* **20**, 155208 (2008).
- [11] C. Gould, C. Rüster, T. Jungwirth, E. Girgis, G. M. Schott, R. Giraud, K. Brunner, G. Schmidt, and L. W. Molenkamp, *Phys. Rev. Lett.* **93**, 117203 (2004).
- [12] C. Rüster, C. Gould, T. Jungwirth, J. Sinova, G. M. Schott, R. Giraud, K. Brunner, G. Schmidt, and L. W. Molenkamp, *Phys. Rev. Lett.* **94**, 027203 (2005).
- [13] J. D. Burton and E. Y. Tsymbal, *Phys. Rev. B* **93**, 024419 (2016).
- [14] B. G. Park, J. Wunderlich, X. Marti, V. Holy, Y. Kurosaki, M. Yamada, H. Yamamoto, A. Nishide, J. Hayakawa, H. Takahashi, A. B. Shick, and T. Jungwirth, *Nat. Mater.* **10**, 347 (2011).
- [15] P. X. Xu, V. M. Karpan, K. Xia, M. Zwierzycki, I. Marushchenko, and P. J. Kelly, *Phys. Rev. B* **73**, 180402(R) (2006).
- [16] H.-M. Tang and K. Xia, *Phys. Rev. Applied* **7**, 034004 (2017).
- [17] A. Matos-Abiague, M. Gmitra, and J. Fabian, *Phys. Rev. B* **80**, 045312 (2009).
- [18] Y. Ke, K. Xia, and H. Guo, *Phys. Rev. Lett.* **105**, 236801 (2010).
- [19] O. Robach, G. Renaud, and A. Barbier, *Phys. Rev. B* **60**, 5858 (1999).
- [20] K. Xia, M. Zwierzycki, M. Talanana, P. J. Kelly, and G. E. W. Bauer, *Phys. Rev. B* **73**, 064420 (2006).
- [21] S. Wang, Y. Xu, and K. Xia, *Phys. Rev. B* **77**, 184430 (2008).
- [22] O. K. Andersen, *Phys. Rev. B* **12**, 3060 (1975).
- [23] O. K. Andersen, Z. Pawłowska, and O. Jepsen, *Phys. Rev. B* **34**, 5253 (1986).
- [24] A. A. Starikov, Y. Liu, Z. Yuan, and P. J. Kelly, *Phys. Rev. B* **97**, 214415 (2018).
- [25] F. L. Zeng, Z. Y. Ren, Y. Li, J. Y. Zeng, M. W. Jia, J. Miao, A. Hoffmann, W. Zhang, Y. Z. Wu, and Z. Yuan, *Phys. Rev. Lett.* **125**, 097201 (2020).
- [26] Y. Dai, Y. W. Zhao, L. Ma, M. Tang, X. P. Qiu, Y. Liu, Z. Yuan, and S. M. Zhou, *Phys. Rev. Lett.* **128**, 247202 (2022).
- [27] T. McGuire and R. Potter, *IEEE Trans. Magn.* **11**, 1018 (1975).
- [28] C. Heiliger, P. Zahn, B. Y. Yavorsky, and I. Mertig, *Phys. Rev. B* **73**, 214441 (2006).
- [29] W. H. Butler, X.-G. Zhang, T. C. Schulthess, and J. M. MacLaren, *Phys. Rev. B* **63**, 054416 (2001).